Accepted Manuscript
Version of Record at: https://doi.org/10.1002/zamm.202300521

A SUPERCONVERGENT CDG FINITE ELEMENT FOR THE POISSON EQUATION ON POLYTOPAL MESHES

XIU YE AND SHANGYOU ZHANG

Abstract. A conforming discontinuous Galerkin (CDG) finite element is constructed for solving second order elliptic equations on polygonal and polyhedral meshes. The numerical trace on the edge between two elements is no longer the average of two discontinuous P_k functions on the two sides, but a lifted P_{k+2} function from four P_k functions. When the the numerical gradient space is the $H(\mathrm{div}, T)$ subspace of piecewise P_{k+1}^d polynomials on subtriangles/subtehrahedra of a polygon/polyhedron T which have a one-piece polynomial divergence on T, this CDG method has a superconvergence of order two above the optimal order. Due to the superconvergence, we define a post-process which lifts a P_k CDG solution to a quasi-optimal P_{k+2} solution on each element. Numerical examples in 2D and 3D are computed and the results confirm the theory.

1. Introduction

A new conforming discontinuous Galerkin finite element method is developed for the second order elliptic problem,

$$-\Delta u = f \quad \text{in } \Omega, \tag{1.1}$$

$$u = 0 \quad \text{on } \partial\Omega, \tag{1.2}$$

where Ω can be subdivided into polygonal meshes in 2D, or polyhedral meshes in 3D.

There are three types of finite element methods for problem (1.1). The continuous Galerkin method solves (1.1) by continuous piecewise P_k polynomials on a triangular or tetrahedral mesh: Find $u_h \in V_h \subset H_0^1(\Omega)$ such that

$$(\nabla u_h, \nabla v_h) = (f, v_h) \quad \forall v_h \in V_h. \tag{1.3}$$

The method is commonly called a conforming finite element method. The nonconforming finite element method employs piecewise P_k polynomials which are continuous weakly on edges only up to order P_{k-1}. The same weak form (1.3) is also used by the nonconforming elements. A third type of finite elements is the discontinuous Galerkin (DG) method, where the finite element space is formed by discontinuous piecewise P_k polynomials. In DG methods, inter-element integral terms and a penalty term are added to the weak form (1.3) in order to control the consistence error and to obtain convergent solutions, cf. [2]. But a conforming discontinuous

1991 *Mathematics Subject Classification.* Primary, 65N15, 65N30.
Key words and phrases. finite element, conforming discontinuous Galerkin method, stabilizer free, polytopal mesh, super-convergent.

Galerkin (CDG) method is introduced in [4, 10, 11, 12, 13, 15, 16, 17, 18] which keeps the weak form (1.3) of the conforming finite element method, unlike the other DG methods.

This paper extends the two-order superconvergent CDG method of [18], which is on triangular and tetrahedral meshes only, to general polytopal meshes in 2D and 3D. Unlike other DG methods, the inter-element trace of discontinuous functions is not the simple average of two functions on the two sides. In this CDG method, the numerical trace is the P_{k+1}-projection of a lifted P_{k+2} polynomial from four P_k functions nearby, or eight P_k functions in 3D.

Additionally we compute the gradient of discontinuous P_k functions on a polygon by its projection in a piecewise P_{k+1}-$H(\text{div})$ space on a triangular subdivision of the polygon. Such P_{k+1}-$H(\text{div})$ spaces are not BDM $H(\text{div})$ spaces on triangular or tetrahedral meshes. They are specially designed so that the divergence is a one-piece P_k polynomial on one polygon or polyhedron. Therefore we limit polygons to one type, and polyhedra to two types, in our polytopal meshes, described in Section 2. But they cover commonly seen polygons and polyhedra. We note that the dimension of such a multi-piece P_{k+1}-$H(\text{div})$ space is big. But the space is used for computing the stiffness matrix only, i.e., for defining a quadrature formula only. For example, for the P_2 CDG on a hexahedron, $\dim V_h = 10$, but for its gradient space, $\dim \Lambda_{k+1} \approx 6 \times 3 \times \dim P_3 = 360$. We need a very large gradient space to catch the jump in P_{k+1} order on the six polygonal faces, so that we can obtain a superconvergent CDG method.

We show that such a CDG solution converges two orders above the optimal order, on polytopal meshes. That is, the error between the L^2 projection of the true solution in P_k on one polygon and the computed CDG P_k solution converges at $O(h^{k+3})$ in L^2-norm, and at $O(h^{k+2})$ in H^1 like-norm. Because of this superconvergence, we post-process such a P_k CDG solution to get a quasi-optimal P_{k+2} solution on each polygon, or polyhedron. Numerical tests are performed in 2D and 3D, confirming the theory.

2. Macro $H(\text{div})$ finite elements on polygonal and polyhedral meshes

2.1. **Polygon.** We limit the polygons in the mesh to one type: It can be subdivided into finite quasi-uniform triangles by connecting one vertex with all rest vertices, cf. Figure 2.1. That is, we do not allow any edge subdivision, neither any other internal subdivision.

Let $T \in \mathcal{T}_h$ be a n-polygon, cf. Figure 2.1. We assume T can be subdivided into $n-2$ shape regular triangles by connecting one vertex $\mathbf{x}_1$ with vertices $\mathbf{x}_3, \ldots, \mathbf{x}_{n-1}$. The polygonal $H(\text{div})$ finite element space $\Lambda_k(T)$ is defined by, $k \geq 1$,

$$\Lambda_k(T) = \left\{ \mathbf{v} = \sum_{l=1}^{\dim \Lambda_k} F_l(\mathbf{v}) \mathbf{v}_l : \ \mathbf{v}|_{T_i} \in [P_k(T_i)]^2 \right\}, \tag{2.1}$$

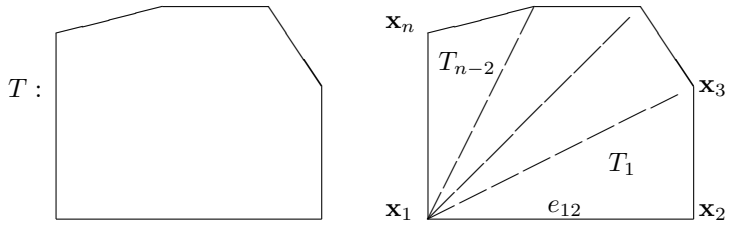

FIGURE 2.1. A polygon is subdivided in to triangles by connecting ONLY one vertex with other vertices.

where the degrees of freedom $\{F_l\}$ are

$$F_l(\mathbf{u}) = \begin{cases} \int_{e_{j,j+1}} \mathbf{u}\cdot\mathbf{n} p ds, & j=1,\ldots,n,\ p\in P_k(e_{j,j+1}),\\ \int_{e_{1j}} \mathbf{u}\cdot\mathbf{n} p ds, & j=3,\ldots,n-1,\ p\in P_k(e_{1j})\setminus P_0,\\ \int_T \mathbf{u}\cdot\nabla p d\mathbf{x}, & p\in P_{k-1}(T)\setminus P_0,\\ \int_{T_j} \mathbf{u}\cdot\nabla^\perp(pB_j) d\mathbf{x}, & j=1,\ldots,n-2,\ p\in P_{k-2}(T_j), \end{cases} \tag{2.2}$$

where edge $e_{j,j+1}=\mathbf{x}_j\mathbf{x}_{j+1}$, $\mathbf{x}_{n+1}=\mathbf{x}_1$, $\mathbf{n}$ is a fixed unit normal vector on the edge, $T_j=\mathbf{x}_1\mathbf{x}_{j+1}\mathbf{x}_{j+2}$, $\nabla^\perp f=\langle -\partial_y f,\partial_x f\rangle$, and $B_j=\lambda_1\lambda_2\lambda_3$ with the barycentric coordinates (i.e., the linear function $\lambda_i=0$ on one edge of the triangle T_j and $\lambda_i=1$ at the opposite vertex.) The numbers of degrees of freedom in the four lines of (2.2) are

$$n,\ n-4,\ k(k+1)/2-1,\ \text{and}\quad (n-2)(k-1)k/2,\ \text{respectively.}$$

In (2.1), $\{\mathbf{v}_l\}$ is the basis dual to $\{F_i\}$, satisfying the following continuity constraints on the functions of $\Lambda_k(T)$,

$$\begin{cases} \int_{e_{1j}} [\mathbf{v}_l]\cdot\mathbf{n} p ds=0, & j=3,\ldots,n-1,\ p\in P_0(e_{1j}),\\ q_j-q_1=0, & j=2,\ldots,n-2, \end{cases} \tag{2.3}$$

where $[\cdot]$ denotes the jump on the edge and polynomial $q_j\in P_{k-1}(T)$ is the natural extension of $\tilde{q}_j=\operatorname{div}\mathbf{v}_l|_{T_j}\in P_{k-1}(T_j)$. The first condition in (2.3) ensures $\mathbf{v}_l\in H(\operatorname{div},T)$. The second condition in (2.3) enforces $\operatorname{div}\mathbf{v}_l\in P_{k-1}(T)$, a one-piece polynomial divergence. We have

$$\Lambda_k(T)\subset\{\mathbf{v}\in H(\operatorname{div},T):\ \mathbf{v}|_{T_i}\in[P_k(T_i)]^2,\ \ \nabla\cdot\mathbf{v}\in P_{k-1}(T)\}.$$

2.2. **Type 1 polyhedron.** The polyhedron can be subdivided into quasi-uniform tetrahedra by connecting one vertex with all other vertices on every face-polygon of the polyhedron, cf. Figure 2.2. That is, no internal edge can be introduced in the subdivision and all face polygons are of the type we accept in the last subsection.

Let T be an m-polygon-face polyhedron, cf. Figure 2.2. Let R_i be a face polygon of T. We subdivide it into f_i (may have $f_i=1$ triangles $\{e_{i,1},\ldots,e_{if_i}\}$. Together we get $M=4n-2(n-1)$ face-triangles, where n is the number of tetrahedra after the subdivision. With these M triangles and no internal edge introduced, we assume T is subdivided into n shape regular tetrahedra, $\{T_1,\ldots,T_n\}$. Between T_i

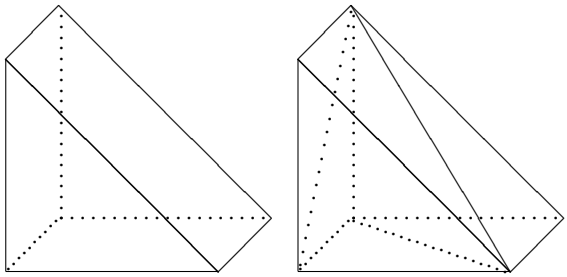

FIGURE 2.2. An m-face ($m = 5$ in the figure) polyhedron is subdivided in to n ($n = 3$) tetrahedra, where there is no internal edge, there are exactly $(n-1)$ internal triangles, a face polygon R_i is subdivided into f_i triangles $\{e_{i1}, \ldots, e_{i,f_i}\}$ ($f_i = 1$ or 2 in the figure), and there are M outside face triangles.

and T_{i+1}, we have one internal triangle t_i. There are $(n-1)$ internal triangles t_i separating the n tetrahedra.

We define the 3D $H(\text{div})$ macro-element space on T as, for $k \geq 1$,

$$\Lambda_k(T) = \{\mathbf{v} = \sum_{l=1}^{\dim \Lambda_k} F_l(\mathbf{v})\mathbf{v}_l \ : \ \mathbf{v}_l|_{T_i} \in [P_k(T_i)]^3\}, \tag{2.4}$$

where the basis $\{\mathbf{v}_l\}$ is dual to the set $\{F_l\}$ of the linear functionals:

$$F_l(\mathbf{u}) = \begin{cases} \int_{e_{i1}} \mathbf{u}\cdot\mathbf{n} p ds, & i = 1, \ldots, m, \ p \in P_k(e_{i1}), \\ \int_{t_i} (\mathbf{u}|_{T_i})\cdot\mathbf{n} p ds, & i = 1, \ldots, n-1, \ p \in P_k(t_i) \setminus P_0(t_i), \\ \int_{T_i} \mathbf{u}\cdot\mathbf{p} d\mathbf{x}, & i = 1, \ldots, n, \ \mathbf{p} \in \mathbf{CP}_k(T_i), \\ \int_T \mathbf{u}\cdot\nabla p d\mathbf{x}, & p \in P_{k-1}(T) \setminus P_0(T). \end{cases} \tag{2.5}$$

Here the curl space is

$$\begin{aligned} \mathbf{CP}_k(T_j) = \{\mathbf{v} \in P_k(T_j)^3 \ : \ & \mathbf{v}\cdot\mathbf{n}|_{\partial T_j} = 0, \\ & \mathbf{v}\cdot\nabla p = 0 \ \forall p \in P_{k-1}(T_j) \setminus P_0(T_j)\}, \end{aligned} \tag{2.6}$$

which has its dimension as

$$\begin{aligned} \dim \mathbf{CP}_k(T_j) &= \frac{3(k+1)(k+2)(k+3)}{6} - \frac{4(k+1)(k+2)}{2} \\ &\quad - \frac{(k)(k+1)(k+2)}{6} + 1 \\ &= \frac{(k+1)(k+2)(2k-3)}{6} + 1. \end{aligned}$$

The numbers of degrees of freedom in the four lines of (2.5) are

$$\begin{aligned} &m(k+1)(k+2)/2, \ (n-1)((k+1)(k+2)/2-1), \\ &n((k+1)(k+2)(2k-3)/6+1), \text{ and } \quad k(k+1)(k+2)/6-1, \text{ respectively.} \end{aligned}$$

Additionally in (2.4), $\{\mathbf{v}_l\}$ satisfy the following constraints,

$$\begin{cases} \int_{e_{i1}} (\mathbf{v}_l - \mathbf{v}_l|_{e_{ij}}) \cdot \mathbf{n} p ds = 0, & i = 1, \ldots, m,\ p \in P_k(e_{ij}), \\ & j = 2, \ldots, i_f, \\ \int_{t_i} [\mathbf{v}_l] \cdot \mathbf{n} p ds = 0, & i = 1, \ldots, n-1,\ p \in P_k(t_i), \\ q_i - q_1 = 0, & j = 2, \ldots, n, \end{cases} \tag{2.7}$$

where $[\mathbf{v}_l]$ is the jump of $\mathbf{v}_l$ at triangle t_i and polynomial $q_j \in P_{k-1}(T)$ is the natural extension of $\tilde{q}_j = \operatorname{div} \mathbf{v}_l|_{T_j} \in P_{k-1}(T_j)$.

2.3. **Type 2 polyhedron.** The polyhedron can be subdivided into quasi-uniform tetrahedra by introducing exactly one internal edge, cf. Figure 2.3. Again, all face polygons of the polyhedron are of the type we accept in the first subsection.

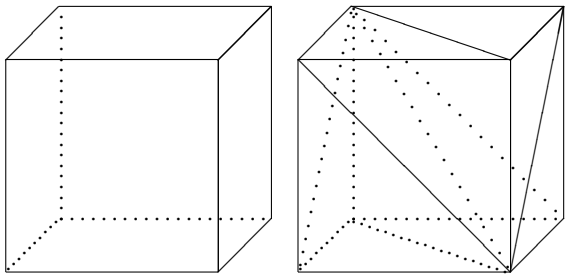

FIGURE 2.3. An m-face ($m = 6$ in the figure) polyhedron is subdivided in to n ($n = 6$) tetrahedra, where there is exactly one internal edge, there are exactly n internal triangles, a face polygon R_i is subdivided into f_i ($f_i = 2$) triangles $\{e_{i1}, \ldots, e_{i,f_i}\}$, and there are M face triangles.

Let $T \in \mathcal{T}_h$ be an m-polygon-face polyhedron, cf. Figure 2.3. Let G_i be a face polygon of T. We subdivide it into f_i triangles $\{e_{i,1}, \ldots, e_{if_i}\}$. Together we get $M = 2n$ face-triangles. With these M triangles and exactly one internal edge (connecting two vertices), we assume T is subdivided into n shape regular tetrahedra, $\{T_1, \ldots, T_n\}$. Between T_i and T_{i+1}, we have one internal triangle t_i. t_n is the triangle between T_n and T_1.

We define the 3D $H(\operatorname{div})$ macro-element space on T as, $k \geq 1$,

$$\Lambda_k(T) = \{\mathbf{v} = \sum_{i=1}^{n} F_l(\mathbf{v}) \mathbf{v}_l \ :\ \mathbf{v}_l|_{T_i} \in [P_k(T_i)]^3\}, \tag{2.8}$$

where the basis $\{\mathbf{v}_l\}$ is dual to the set $\{F_l\}$ of the linear functionals,

$$F_l(\mathbf{u}) = \begin{cases} \int_{e_{i1}} \mathbf{u} \cdot \mathbf{n} p ds, & i = 1, \ldots, m,\ p \in P_k(e_{i1}), \\ \int_{t_i} (\mathbf{u}|_{T_i}) \cdot \mathbf{n} p ds, & i = 1, \ldots, n,\ p \in P_k(t_i) \setminus P_0(t_i), \\ \int_{t_1} (\mathbf{u}|_{T_1}) \cdot \mathbf{n} p ds, & p \in P_0(t_1), \\ \int_{T_i} \mathbf{u} \cdot \mathbf{p} d\mathbf{x}, & i = 1, \ldots, n,\ \mathbf{p} \in \mathbf{CP}_k(T_i), \\ \int_T \mathbf{u} \cdot \nabla p d\mathbf{x}, & p \in P_{k-1}(T) \setminus P_0(T). \end{cases} \tag{2.9}$$

Here the curl space $\mathbf{CP}_k(T_i)$ is defined in (2.6), and t_1 is an internal triangle which is on a tetrahedron having two other face-triangles on ∂T. The numbers of degrees of freedom in the five lines of (2.9) are

$$m(k+1)(k+2)/2,\ n((k+1)(k+2)/2-1),\ 1,$$
$$n((k+1)(k+2)(2k-3)/6+1),\ \text{and}\quad k(k+1)(k+2)/6-1,\ \text{respectively.}$$

In addition, $\{\mathbf{v}_l\}$ in (2.8) satisfy the continuity constraints:

$$\begin{cases} \int_{e_{i1}} (\mathbf{v}_l - \mathbf{v}_l|_{e_{ij}}) \cdot \mathbf{n} p ds = 0, & i=1,\ldots,m,\ p\in P_k(e_{ij}), \\ & j=2,\ldots,i_f, \\ \int_{t_i} [\mathbf{v}_l]\cdot \mathbf{n} p ds = 0, & i=1,\ldots,n,\ p\in P_k(t_i), \\ q_j - q_1 = 0, & j=2,\ldots,n, \end{cases} \tag{2.10}$$

where $[\mathbf{v}_l]$ is the jump of $\mathbf{v}_l$ at triangle t_i and polynomial $q_j \in P_{k-1}(T)$ is the natural extension of $\tilde{q}_j = \operatorname{div} \mathbf{v}_l|_{T_j} \in P_{k-1}(T_j)$.

3. CDG Finite Element Scheme

Let $\mathcal{T}_h$ be a partition of the domain Ω consisting of polygons/polyhedra. The allowed polygons and polyhedra are defined in last section. For every element $T \in \mathcal{T}_h$, we denote by h_T its diameter and by $h = \max_{T\in\mathcal{T}_h} h_T$ for $\mathcal{T}_h$. Denote by $\mathcal{E}_h$ the set of all edges/face-triangles in $\mathcal{T}_h$, and by $\mathcal{E}_h^0 = \mathcal{E}_h \backslash \partial\Omega$ the set of all interior edges/face-triangles.

Let Π_k and Π_k^b be the generic local L^2 projections onto $[P_k(T)]^j$ for $T \in \mathcal{T}_h$ and $[P_k(e)]^j$ for $e \in \mathcal{E}_h$ respectively where $j = 1, \cdots, d$.

For the purpose of analysis, we introduce a local weak Galerkin finite element space $W(T)$ as, cf. [3, 5, 7, 8, 9, 19] for some references on the weak Galerkin finite element method,

$$W(T) = \{v = \{v_0, v_b\} \in P_k(T) \times P_{k+1}(\mathcal{E}_h)\ :\ v_b|_e \in P_{k+1}(e),\ e \subset \partial T\}. \tag{3.1}$$

For any $v = \{v_0, v_b\} \in W(T)$, its weak gradient $\nabla_w v \in \Lambda_{k+1}(T)$ is defined as the unique solution of the following equation,

$$(\nabla_w v, \mathbf{q})_T = -(v_0, \nabla\cdot\mathbf{q})_T + \langle v_b, \mathbf{q}\cdot\mathbf{n}\rangle_{\partial T} \qquad \forall \mathbf{q} \in \Lambda_{k+1}(T), \tag{3.2}$$

where the vector space $\Lambda_{k+1}(T)$ is defined in (2.1), or (2.4) or (2.8), depending on the polygon or polyhedron type.

Theorem 3.1 ([6, 14]). *For $\tau \in H^{k+2}(\Omega)^d$, there exists a projection Π_h with $\Pi_h\tau \in H(\operatorname{div},\Omega)$ satisfying $\Pi_h\tau|_T \in \Lambda_{k+1}(T)$ and*

$$(\nabla\cdot\tau,\ v_0)_T = (\nabla\cdot\Pi_h\tau,\ v_0)_T \quad \forall v_h = \{v_0, v_b\} \in W(T), \tag{3.3}$$

$$-(\nabla\cdot\tau,\ v_0)_{\mathcal{T}_h} = (\Pi_h\tau,\ \nabla_w v_h)_{\mathcal{T}_h} \quad \forall v_h = \{v_0, v_b\} \in W(T),\ T \in \mathcal{T}_h, \tag{3.4}$$

$$\|\Pi_h\tau - \tau\|_0 \le Ch^{k+2}|\tau|_{k+2}, \tag{3.5}$$

where the weak gradient $\nabla_w v_h$ is defined in (3.2).

For $T \in \mathcal{T}_h$, we define a local CDG element $V(T)$ as,

$$V(T) = \{v \in H^1(T) :\ v|_T \in P_k(T)\}. \tag{3.6}$$

To connect the vector spaces $V(T)$ and $W(T)$, we define an embedding operator $E_h : V(T) \to W(T)$ such that for $v \in V(T)$

$$E_h v = \{v, \Pi_{k+1}^b E_e v\} \in W(T), \tag{3.7}$$

where Π_{k+1}^b is the L^2 projection on edge e and $E_e \in P_{k+2}(U_e)$ is defined by

$$\begin{cases} E_e v = 0, & \text{if } e \subset \partial\Omega, \\ (E_e v, \Pi_k w)_{S_e} = (v, \Pi_k w)_{S_e} \ \forall w \in P_{k+2}(U_e), & \text{if } e \in \mathcal{E}_h^0. \end{cases} \tag{3.8}$$

Here Π_k is a local L^2-projection on to space $\prod_{i=1}^4 P_k(S_i)$, S_e is a union (with the center (x_c, y_c)) of 4 aligned squares $\{S_i\}$ inside U_e,

$$\begin{aligned} S_1 &= [x_c - \frac{5}{4}\gamma_0 h, x_c - \frac{3}{4}\gamma_0 h] \times [y_c - \frac{5}{4}\gamma_0 h, y_c - \frac{3}{4}\gamma_0 h], \\ S_2 &= [x_c + \frac{3}{4}\gamma_0 h, x_c + \frac{5}{4}\gamma_0 h] \times [y_c - \frac{5}{4}\gamma_0 h, y_c - \frac{3}{4}\gamma_0 h], \\ S_3 &= [x_c + \frac{3}{4}\gamma_0 h, x_c + \frac{5}{4}\gamma_0 h] \times [y_c + \frac{3}{4}\gamma_0 h, y_c + \frac{5}{4}\gamma_0 h], \\ S_4 &= [x_c - \frac{5}{4}\gamma_0 h, x_c - \frac{3}{4}\gamma_0 h] \times [y_c + \frac{3}{4}\gamma_0 h, y_c + \frac{5}{4}\gamma_0 h], \end{aligned}$$

for some fixed $\gamma_0 > 0$, and U_e is a union of polygons containing the four aligned squares, cf. Figure 3.1. Here four aligned squares may rotate together. [18] proves that (3.8) defines an $E_e v$. [18] shows also that it preserves $P_{k+2}(U_e)$ polynomials in the sense $E_e v = w$ if $v|_{S_i} = \Pi_{k,S_e} w$ for all $w \in P_{k+2}(U_e)$. In 3D, the set $\{S_i\}$ in (3.8) contains eight aligned cubes, two in each direction.

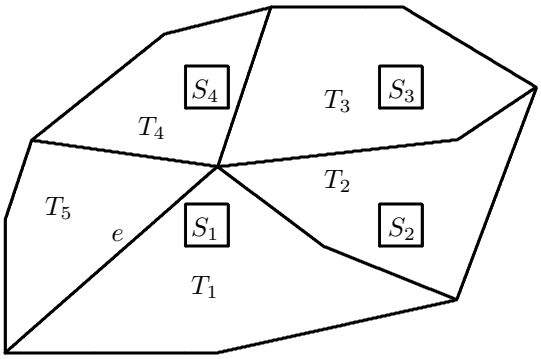

FIGURE 3.1. A closed polygon $U_e = \cup_{i=1}^{n_e} T_i$ contains 4 aligned squares, for an edge e, where $n_e = 5$ and T_i is a closed triangle.

Lemma 3.1 ([18]). *For $k \geq 1$, the lifting operator $E_e : V_h \to P_{k+2}(U_e)$, defined in* (3.8)*, has an order $k+2$ accuracy, i.e., for any $u \in H^{k+3}(\Omega)$,*

$$\|E_e \Pi_k u - u\|_{0,U_e} + h\|\nabla(E_e \Pi_k u - u)\|_{0,U_e} \leq C h^{k+3} |u|_{k+3,U_e}. \tag{3.9}$$

Since $E_h v \in W(T)$, $\nabla_w E_h v$ can be calculated by (3.2). For $v \in V(T)$, its weak gradient $\nabla_w v$ is defined as

$$\nabla_w v = \nabla_w E_h v. \tag{3.10}$$

For a given integer $k \geq 1$, let V_h be the CDG finite element space associated with $\mathcal{T}_h$ by

$$V_h = \{v \in L^2(\Omega) : \ v|_T \in V(T), \ T \in \mathcal{T}_h\}. \tag{3.11}$$

The CDG finite element method is to find $u_h \in V_h$ such that

$$(\nabla_w u_h, \nabla_w v) = (f, v) \quad \forall v \in V_h. \tag{3.12}$$

4. Well posedness

We start this section by defining two semi-norms as follows for $v|_T = \{v_0, v_b\} \in W(T)$,

$$|||v|||^2 = (\nabla_w v, \nabla_w v), \tag{4.1}$$

$$\|v\|_{1,h}^2 = \sum_{T \in \mathcal{T}_h} (\|\nabla v_0\|_T^2 + h_T^{-1}\|v_0 - v_b\|_{\partial T}^2). \tag{4.2}$$

For $v \in V_h$, we define

$$|||v||| = |||E_h v|||, \tag{4.3}$$

$$\|v\|_{1,h} = \|E_h v\|_{1,h}. \tag{4.4}$$

Lemma 4.1. *$\|v\|_{1,h}$ defines a norm in V_h.*

Proof. We just need to show that if $\|v\|_{1,h} = 0$, $v = 0$ for any $v \in V_h$. Now we assume $\|v\|_{1,h} = 0$, which implies

$$0 = \|v\|_{1,h}^2 = \|E_h v\|_{1,h}^2 = \sum_{T \in \mathcal{T}_h} (\|\nabla v\|_T^2 + h_T^{-1}\|v - v_b\|_{\partial T}^2),$$

where v_b is defined in (3.8). Thus we have that $\nabla v = 0$ on $T \in \mathcal{T}_h$ and $v = v_b$ on $e \in \mathcal{E}_h$. Thus we have that v is a constant over Ω. By (3.8), we have $v = v_b = 0$ on $\partial\Omega$. The lemma is proved. □

Lemma 4.2 ([14])**.** *The two norms defined in (4.3) and (4.4) are equivalent,*

$$C_1\|v\|_{1,h} \leq |||v||| \leq C_2\|v\|_{1,h} \quad \forall v \in V_h. \tag{4.5}$$

The two lemmas above imply the well posedness of the CDG method.

Lemma 4.3. *The CDG finite element method* (3.12) *has a unique solution.*

5. Error equation

Let Q_h be a projection operator such that $Q_h u|_T = \{\Pi_k u, \Pi_{k+1}^b u\} \in W(T)$ on $T \in \mathcal{T}_h$.

Lemma 5.1. *Let $\phi \in H^1(T)$, then one has*

$$\nabla_w Q_h \phi = \Pi_{k+1} \nabla \phi. \tag{5.1}$$

Proof. It follows from (3.2) that for any $\mathbf{q} \in [P_{k+1}(T)]^d$,

$$\begin{aligned}(\nabla_w Q_h\phi, \mathbf{q})_T &= -(\Pi_k\phi, \nabla\cdot\mathbf{q})_T + \langle \Pi_{k+1}^b\phi, \mathbf{q}\cdot\mathbf{n}\rangle_{\partial T}\\ &= -(\phi, \nabla\cdot\mathbf{q})_T + \langle \phi, \mathbf{q}\cdot\mathbf{n}\rangle_{\partial T}\\ &= (\nabla\phi, \mathbf{q})_T = (\Pi_{k+1}\nabla\phi, \mathbf{q})_T,\end{aligned}$$

which proves the lemma. □

Let $e_h = Q_h u - E_h u_h$ with E_h defined in (3.7). Next we derive an error equation for e_h.

Lemma 5.2. *For any $v \in V_h$, one has,*

$$(\nabla_w e_h, \nabla_w v) \quad = \quad \ell_1(u, v), \tag{5.2}$$

where

$$\ell_1(u, v) \quad = \quad \langle (\nabla u - \Pi_{k+1}\nabla u)\cdot\mathbf{n}, v - v_b\rangle_{\partial\mathcal{T}_h}.$$

Proof. For the v_b defined in (3.8), we have

$$\sum_{T\in\mathcal{T}_h} \langle \nabla u\cdot\mathbf{n}, v_b\rangle_{\partial T} = 0. \tag{5.3}$$

Testing (1.1) by $v \in V_h$, using integration by parts and (5.3), we arrive at

$$(\nabla u, \nabla v)_{\mathcal{T}_h} - \langle \nabla u\cdot\mathbf{n}, v - v_b\rangle_{\partial\mathcal{T}_h} = (f, v). \tag{5.4}$$

It follows from integration by parts, (3.2) and (5.1) that

$$\begin{aligned}(\nabla u, \nabla v)_{\mathcal{T}_h} &= (\Pi_{k+1}\nabla u, \nabla v)_{\mathcal{T}_h}\\ &= -(v, \nabla\cdot(\Pi_{k+1}\nabla u))_{\mathcal{T}_h} + \langle v, \Pi_{k+1}\nabla u\cdot\mathbf{n}\rangle_{\partial\mathcal{T}_h}\\ &= (\Pi_{k+1}\nabla u, \nabla_w v)_{\mathcal{T}_h} + \langle v - v_b, \Pi_{k+1}\nabla u\cdot\mathbf{n}\rangle_{\partial\mathcal{T}_h}\\ &= (\nabla_w Q_h u, \nabla_w v)_{\mathcal{T}_h} + \langle v - v_b, \Pi_{k+1}\nabla u\cdot\mathbf{n}\rangle_{\partial\mathcal{T}_h}. \qquad (5.5)\end{aligned}$$

Using (5.4) and (5.5), we have

$$(\nabla_w Q_h u, \nabla_w v) \quad = \quad (f, v) + \ell_1(u, v). \tag{5.6}$$

The error equation (5.2) follows from subtracting (3.12) from (5.6),

$$(\nabla_w e_h, \nabla_w v) = \ell_1(u, v) \quad \forall v \in V_h,$$

which completes the proof of the lemma. □

6. Error estimate in energy norm

Lemma 6.1. *Let $u \in H^{k+3}(\Omega)$. Then we have*

$$|\!|\!| Q_h u - \Pi_k u |\!|\!| \le C h^{k+2} |u|_{k+3}. \tag{6.1}$$

Proof. Recall $Q_h u = \{\Pi_k u, \Pi_{k+1}^b u\}$ and $E_h \Pi_k u = \{\Pi_k u, \Pi_{k+1}^b E_b \Pi_k u\}$. Letting $q = \nabla_w (Q_h u - \Pi_k u)$ in (3.2) and using the trace, inverse inequality and (3.9) yield

$$\begin{aligned}
&|\!|\!| Q_h - \Pi_k u |\!|\!|^2 = |\!|\!| Q_h u - E_h \Pi_k u |\!|\!|^2 \\
&= \sum_{T\in T_h} \langle \Pi_{k+1}^b u - \Pi_{k+1}^b E_b \Pi_k u, q\rangle_{\partial T} = \sum_{T\in T_h} \langle u - E_b \Pi_k u, q\rangle_{\partial T} \\
&\le \Big(\sum_{T\in T_h} h_T^{-1} \|u - E_b \Pi_k u\|_{0,\partial T}^2 \Big)^{1/2} \Big(\sum_{T\in T_h} h_T \|q\|_{0,\partial T}^2 \Big)^{1/2} \\
&\le C \Big(\sum_{T\in T_h} h_T^{-2} \|u - E_b \Pi_k u\|_{0,T}^2 + \|\nabla (u - E_b \Pi_k u)\|_{0,T}^2 \Big)^{1/2} \|q\|_0 \\
&\le C h^{k+2} |u|_{k+3} |\!|\!| Q_h u - \Pi_k u |\!|\!|.
\end{aligned}$$

We complete the proof of the lemma. □

Lemma 6.2. *For any $w \in H^{k+3}(\Omega)$ and $v \in V_h$, we have*

$$|\ell_1(w, v)| \quad \le \quad C h^{k+2} |w|_{k+3} |\!|\!| v |\!|\!|. \tag{6.2}$$

Proof. Using the Cauchy-Schwarz inequality, the trace inequality and (4.5), we have

$$\begin{aligned}
|\ell_1(w, v)| &= \left| \sum_{T\in \mathcal{T}_h} \langle (\nabla w - \Pi_{k+1} \nabla w) \cdot \mathbf{n}, v - v_b \rangle_{\partial T} \right| \\
&\le C \sum_{T\in \mathcal{T}_h} \|\nabla w - \Pi_{k+1} \nabla w\|_{\partial T} \|v - v_b\|_{\partial T} \\
&\le C \left(\sum_{T\in \mathcal{T}_h} h_T \|(\nabla w - \Pi_{k+1} \nabla w)\|_{\partial T}^2 \right)^{\frac{1}{2}} \left(\sum_{T\in \mathcal{T}_h} h_T^{-1} \|v - v_b\|_{\partial T}^2 \right)^{\frac{1}{2}} \\
&\le C h^k |w|_{k+3} |\!|\!| v |\!|\!|.
\end{aligned}$$

We have proved the lemma. □

Theorem 6.1. *Let $u_h \in V_h$ be the finite element solution of (3.12). Assume the exact solution $u \in H^{k+3}(\Omega)$. Then, there exists a constant C such that*

$$|\!|\!| \Pi_k u - u_h |\!|\!| \quad \le \quad C h^{k+2} |u|_{k+3}. \tag{6.3}$$

Proof. Letting $\epsilon_h = \Pi_k u - u_h \in V_h$ and using (5.2), (6.1) and (6.2) give

$$\begin{aligned}
|\!|\!| \epsilon_h |\!|\!|^2 &= (\nabla_w \epsilon_h, \nabla_w (\Pi_k u - Q_h u)) + (\nabla_w \epsilon_h, \nabla_w e_h) \\
&= (\nabla_w \epsilon_h, \nabla_w (\Pi_k u - Q_h u)) + \ell_1(u, \epsilon_h) \\
&= |\!|\!| \epsilon_h |\!|\!| |\!|\!| \Pi_k u - Q_h u |\!|\!| + \ell_1(u, \epsilon_h) \\
&\le C h^{k+2} |u|_{k+3} |\!|\!| \epsilon_h |\!|\!|. \qquad (6.4)
\end{aligned}$$

We complete the proof of the theorem. □

7. Superconvergence in L2 norm

We use the duality argument to obtain superconvergence of the CDG finite element solution in the L^2 norm. Recall

$$e_h = Q_h u - E_h u_h = \{e_0, e_b\} = \{\Pi_k u - u_h, \Pi_{k+1}^b u - u_b\},$$

where u_b defined in (3.8). The corresponding dual problem seeks $w \in H_0^1(\Omega)$ satisfying

$$-\Delta \Phi = e_0 \quad \text{in } \Omega. \tag{7.1}$$

Assume that the following H^2-regularity holds

$$\|\Phi\|_2 \leq C\|e_0\|_0. \tag{7.2}$$

In the next theorem, we will prove the order two superconvergence of the CDG solution in the L^2-norm.

Theorem 7.1. *Let $u \in H^{k+3}(\Omega) \cap H_0^1(\Omega)$ be the exact solution of (1.1). Let $u_h \in V_h$ be the CDG solution of (3.12). Then*

$$\|\Pi_k u - u_h\|_0 \leq Ch^{k+3}|u|_{k+3}. \tag{7.3}$$

Proof. Testing (7.1) by $e_0 = \Pi_k u - u_h$ and using the fact that $\sum_{T\in\mathcal{T}_h}\langle \nabla\Phi\cdot\mathbf{n}, e_b\rangle_{\partial T} = 0$, (3.2) and (5.1) give

$$\begin{aligned}
\|e_0\|_0^2 &= -(\Delta\Phi, e_0) = (\nabla\Phi,\ \nabla e_0)_{\mathcal{T}_h} - \langle \nabla\Phi\cdot\mathbf{n},\ e_0 - e_b\rangle_{\partial T_h} \\
&= (\Pi_{k+1}\nabla\Phi,\ \nabla e_0)_{\mathcal{T}_h} - \langle \nabla\Phi\cdot\mathbf{n},\ e_0 - e_b\rangle_{\partial T_h} \\
&= -(\nabla\cdot\Pi_{k+1}\nabla\Phi,\ e_0)_{\mathcal{T}_h} + \langle \Pi_{k+1}\nabla\Phi\cdot\mathbf{n},\ e_0\rangle_{\partial T_h} \\
&- \langle \nabla\Phi\cdot\mathbf{n},\ e_0 - e_b\rangle_{\partial T_h} \\
&= (\Pi_{k+1}\nabla\Phi,\ \nabla_w e_h) + \langle \Pi_{k+1}\nabla\Phi\cdot\mathbf{n},\ e_0 - e_b\rangle_{\partial T_h} \\
&- \langle \nabla\Phi\cdot\mathbf{n},\ e_0 - e_b\rangle_{\partial T_h} \\
&= (\nabla_w Q_h\Phi,\ \nabla_w e_h) - \ell_1(\Phi, e_h) \\
&= (\nabla_w \Pi_k\Phi,\ \nabla_w e_h) + (\nabla_w(Q_h\Phi - \Pi_k\Phi),\ \nabla_w e_h)_{\mathcal{T}_h} - \ell_1(\Phi, e_h) \\
&= \ell_1(u, \Pi_k\Phi) + (\nabla_w(Q_h\Phi - \Pi_k\Phi),\ \nabla_w e_h)_{\mathcal{T}_h} - \ell_1(\Phi, e_h),
\end{aligned}$$

which implies

$$\|e_0\|_0^2 = \ell_1(u, \Pi_k\Phi) + (\nabla_w(Q_h\Phi - \Pi_k\Phi),\ \nabla_w e_h) - \ell_1(\Phi, e_h). \tag{7.4}$$

Next we will estimate all the terms on the right hand side of (7.4). Using the Cauchy-Schwarz inequality, the trace inequality, we obtain

$$\begin{aligned}
&|\ell_1(u, \Pi_k\Phi)| \\
\leq\ & |\langle (\nabla u - \Pi_{k+1}\nabla u)\cdot\mathbf{n},\ \Pi_k\Phi - E_b\Pi_k\Phi\rangle_{\partial T_h}| \\
\leq\ & C\left(\sum_{T\in\mathcal{T}_h} h\|(\nabla u - \Pi_{k+1}\nabla u)\|_{\partial T}^2\right)^{1/2}\left(\sum_{T\in\mathcal{T}_h} h^{-1}\|\Pi_k\Phi - E_b\Pi_k\Phi\|_{\partial T}^2\right)^{1/2} \\
\leq\ & Ch^{k+3}|u|_{k+3}\|\Phi\|_2.
\end{aligned}$$

The estimate (6.1) and (6.3) imply

$$\begin{aligned} |(\nabla_w(Q_h\Phi - \Pi_k\Phi),\ \nabla_w e_h)| &\leq |\!|\!| Q_h\Phi - \Pi_k\Phi |\!|\!| |\!|\!| e_h |\!|\!| \\ &\leq |\!|\!| Q_h\Phi - \Pi_k\Phi |\!|\!| (|\!|\!| \epsilon_h |\!|\!| + |\!|\!| Q_h u - \Pi_k u |\!|\!|) \\ &\leq Ch^{k+3}|u|_{k+3}\|\Phi\|_2. \end{aligned}$$

Using the trace inequality, (6.1) and (6.3), we obtain

$$\begin{aligned} |\ell_1(\Phi, e_h)| &= \left| \sum_{T\in\mathcal{T}_h} \langle (\Pi_{k+1}\nabla\Phi - \nabla\Phi)\cdot\mathbf{n},\ e_0 - e_b\rangle_{\partial T} \right| \\ &\leq \sum_{T\in\mathcal{T}_h} h_T^{1/2}\|\Pi_{k+1}\nabla\Phi - \nabla\Phi\|_{\partial T} h_T^{-1/2}\|e_0 - e_b\|_{\partial T} \\ &\leq Ch\|\Phi\|_2 |\!|\!| e_h |\!|\!| \\ &\leq Ch\|\Phi\|_2 (|\!|\!| \epsilon_h |\!|\!| + |\!|\!| Q_h u - \Pi_k u |\!|\!|) \\ &\leq Ch^{k+3}|u|_{k+3}\|\Phi\|_2. \end{aligned}$$

Combining all the estimates above with (7.4) yields

$$\|e_0\|_0^2 \leq Ch^{k+1}|u|_{k+1}\|\Phi\|_2.$$

The estimate (7.3) follows from the above inequality and the regularity assumption (7.2). We have completed the proof. □

8. A locally lifted P_{k+2} solution

Using the superconvergent P_k solution u_h (to the L^2-projection of u) and its superconvergent weak gradient, we reconstruct a quasi-optimal P_{k+2} solution $\hat{u}$ on each polygon/polyhedron.

On each element T, we solve a local problem that finds $\hat{u}_h \in P_{k+2}(T)$ by

$$(\nabla\hat{u}_h - \nabla_w u_h, \nabla v)_T = 0 \quad \forall v \in P_{k+2}(T)\setminus P_0(T), \tag{8.1}$$

$$(\hat{u}_h - u_h, v)_T = 0 \quad \forall v \in P_0(T). \tag{8.2}$$

Theorem 8.1. *Let $u \in H_0^1(\Omega)\cap H^{k+3}(\Omega)$ be the exact solution of (1.1)–(1.2). Let $\hat{u}_h \in \Pi_{T\in\mathcal{T}_h} P_{k+2}(T)$ be the locally lifted solution of (8.1)–(8.2). Then there exists a constant C such that*

$$\|u - \hat{u}_h\|_0 \leq Ch^{k+3}|u|_{k+3}. \tag{8.3}$$

Proof. It is straightforward to show that (8.1)-(8.2) has a unique solution, cf. [18].

As the estimate (8.3) is equation independent, by (6.3) and (7.3), the theorem is proved as in [18]. □

9. Numerical Experiments

We solve the Poisson problem (1.1)–(1.2) on the unit square domain $(0,1)\times(0,1)$ with the exact solution

$$u = \sin(\pi x)\sin(\pi y). \tag{9.1}$$

We compute the solution (9.1) on a type of quadrilateral grids, shown in Figure 9.1. To avoid the convergence to parallelograms under the nest refinement, we fix the shape of quadrilaterals on all levels of grids. We list the computational results in Tables 9.1–9.3. We have two orders of superconvergence in L^2-norm and in H^1-like norm for all order finite elements. Additionally the P_k CDG solution is lifted to get an optimal order P_{k+2} solution.

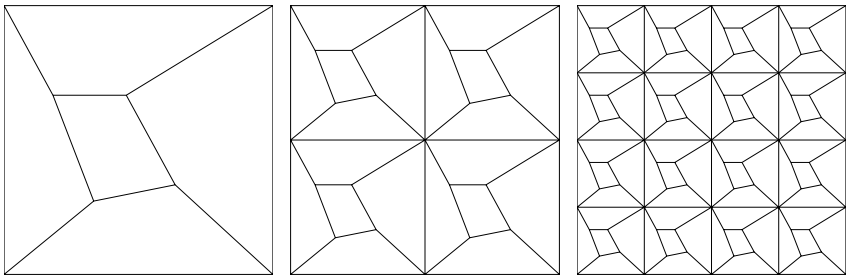

FIGURE 9.1. The first three levels of quadrilateral grids, for Tables 9.1–9.3.

TABLE 9.1. Error profiles and convergence rates on quadrilateral grids shown in Figure 9.1 for (9.1).

level	$\|\Pi_k u - u_h\|_0$	rate	$\|\!\|\!\|\Pi_k u - u_h\|\!\|\!\|$	rate
	by the P_1 CDG finite element			
5	0.1348E-05	4.01	0.4107E-03	2.96
6	0.8431E-07	4.00	0.5213E-04	2.98
7	0.5279E-08	4.00	0.6567E-05	2.99
level	$\|u - u_h\|_0$	rate	$\|u - \hat{u}_h\|_0$	rate
	by the P_1 CDG solution and its P_3 lift			
5	0.7358E-03	2.00	0.1834E-05	4.00
6	0.1838E-03	2.00	0.1148E-06	4.00
7	0.4595E-04	2.00	0.7187E-08	4.00

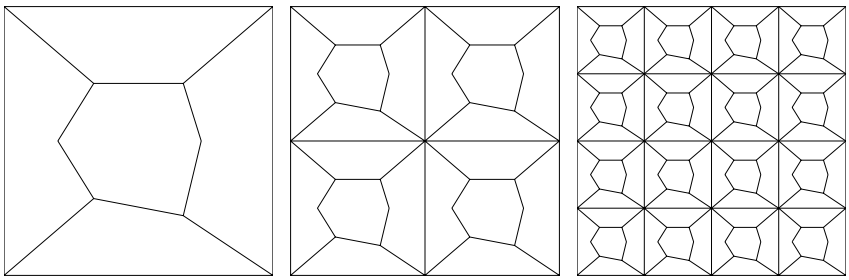

FIGURE 9.2. The first three levels of quadrilateral-pentagon-hexagon grids, for Tables 9.4–9.6.

Next we solve the same problem (9.1) on a type of grids with quadrilaterals, pentagons and hexagons, shown in Figure 9.2. We list the result of computation in

Accepted Manuscript
Version of Record at: https://doi.org/10.1002/zamm.202300521

TABLE 9.2. Error profiles and convergence rates on quadrilateral grids shown in Figure 9.1 for (9.1).

level	$\|\Pi_k u - u_h\|_0$	rate	$\|\|\|\Pi_k u - u_h\|\|\|$	rate
	by the P_2 CDG finite element			
4	0.1137E-05	4.96	0.4991E-03	3.88
5	0.3599E-07	4.98	0.3246E-04	3.94
6	0.1131E-08	4.99	0.2070E-05	3.97
level	$\|u - u_h\|_0$	rate	$\|u - \hat{u}_h\|_0$	rate
	by the P_2 CDG solution and its P_4 lift			
4	0.2226E-03	2.99	0.1260E-05	4.96
5	0.2786E-04	3.00	0.3983E-07	4.98
6	0.3484E-05	3.00	0.1251E-08	4.99

TABLE 9.3. Error profiles and convergence rates on quadrilateral grids shown in Figure 9.1 for (9.1).

level	$\|\Pi_k u - u_h\|_0$	rate	$\|\|\|\Pi_k u - u_h\|\|\|$	rate
	by the P_3 CDG finite element			
3	0.3162E-05	5.87	0.1275E-02	4.76
4	0.5128E-07	5.95	0.4226E-04	4.91
5	0.1670E-08	4.94	0.1355E-05	4.96
level	$\|u - u_h\|_0$	rate	$\|u - \hat{u}_h\|_0$	rate
	by the P_3 CDG solution and its P_5 lift			
3	0.2089E-03	3.98	0.3282E-05	5.87
4	0.1310E-04	3.99	0.5310E-07	5.95
5	0.8194E-06	4.00	0.1684E-08	4.98

Tables 9.4–9.6, where all theoretic supconvergence results are matched. The meshes in Figure 9.2 may look like worse than the quadrilateral meshes in Figure 9.1. But the results are slightly better.

TABLE 9.4. Error profiles and convergence rates on quadrilateral-pentagon-hexagon grids shown in Figure 9.2 for (9.1).

level	$\|\Pi_k u - u_h\|_0$	rate	$\|\|\|\Pi_k u - u_h\|\|\|$	rate
	by the P_1 CDG finite element			
5	0.1265E-05	4.01	0.3882E-03	2.96
6	0.7915E-07	4.00	0.4924E-04	2.98
7	0.4954E-08	4.00	0.6199E-05	2.99
level	$\|u - u_h\|_0$	rate	$\|u - \hat{u}_h\|_0$	rate
	by the P_1 CDG solution and its P_3 lift			
5	0.5942E-03	2.00	0.1676E-05	4.00
6	0.1484E-03	2.00	0.1049E-06	4.00
7	0.3710E-04	2.00	0.6562E-08	4.00

TABLE 9.5. Error profiles and convergence rates on quadrilateral-pentagon-hexagon grids shown in Figure 9.2 for (9.1).

level	$\|\Pi_k u - u_h\|_0$	rate	$\|\|\|\Pi_k u - u_h\|\|\|$	rate
	by the P_2 CDG finite element			
4	0.9371E-06	4.92	0.3746E-03	3.84
5	0.3006E-07	4.96	0.2473E-04	3.92
6	0.9546E-09	4.98	0.1585E-05	3.96
level	$\|u - u_h\|_0$	rate	$\|u - \hat{u}_h\|_0$	rate
	by the P_2 CDG solution and its P_4 lift			
4	0.1595E-03	2.99	0.1054E-05	4.93
5	0.1997E-04	3.00	0.3367E-07	4.97
6	0.2498E-05	3.00	0.1066E-08	4.98

TABLE 9.6. Error profiles and convergence rates on quadrilateral-pentagon-hexagon grids shown in Figure 9.2 for (9.1).

level	$\|\Pi_k u - u_h\|_0$	rate	$\|\|\|\Pi_k u - u_h\|\|\|$	rate
	by the P_3 CDG finite element			
3	0.2075E-05	5.80	0.4532E-03	4.60
4	0.3416E-07	5.92	0.1552E-04	4.87
5	0.6375E-09	5.74	0.5048E-06	4.94
level	$\|u - u_h\|_0$	rate	$\|u - \hat{u}_h\|_0$	rate
	by the P_3 CDG solution and its P_5 lift			
3	0.1260E-03	3.98	0.2229E-05	5.81
4	0.7910E-05	3.99	0.3655E-07	5.93
5	0.4951E-06	4.00	0.6695E-09	5.77

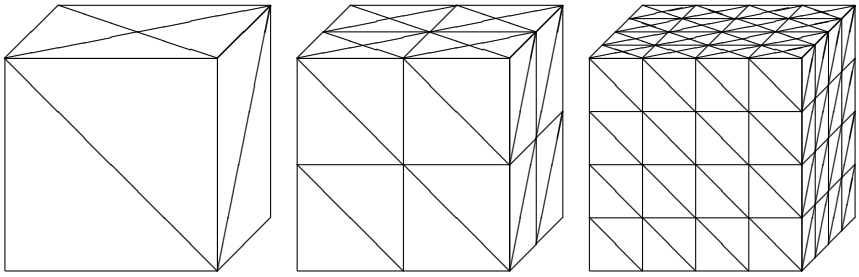

FIGURE 9.3. The first three levels of grids used in Tables 9.7–9.9.

We solve a 3D problem (1.1)–(1.2) on the unit cube domain $\Omega = (0,1)^3$ with the exact solution

$$u = x(1-x)y(1-y)z(1-z^2). \tag{9.2}$$

Here we use a type of tetrahedral grids, shown in Figure 9.3. Here each cube is subdivided in to 16 tetrahedrons with four rectangular faces being cut into two triangles and two rectangular faces (top and bottom) being cut into four triangles. The results are listed in Tables 9.7–9.9, confirming the two-order superconvergence in the two norms for all polynomial-degree $k \geq 1$ elements.

TABLE 9.7. Error profile for solving (9.2) on 3D grids shown in Figure 9.3.

level	$\|\Pi_k u - u_h\|_0$	rate	$\|\|\|\Pi_k u - u_h\|\|\|$	rate
	by the P_1 CDG finite element			
4	0.1118E-05	4.23	0.1799E-03	2.90
5	0.6650E-07	4.07	0.2334E-04	2.95
6	0.4111E-08	4.02	0.2975E-05	2.97
level	$\|u - u_h\|_0$	rate	$\|u - \hat{u}_h\|_0$	rate
	by the P_1 CDG solution and its P_3 lift			
4	0.4903E-04	2.06	0.3719E-06	4.12
5	0.1218E-04	2.01	0.2318E-07	4.00
6	0.3043E-05	2.00	0.1432E-08	4.02

TABLE 9.8. Error profile for solving (9.2) on 3D grids shown in Figure 9.3.

level	$\|\Pi_k u - u_h\|_0$	rate	$\|\|\|\Pi_k u - u_h\|\|\|$	rate
	by the P_2 CDG finite element			
2	0.7642E-04	3.82	0.3329E-02	2.83
3	0.2316E-05	5.04	0.2514E-03	3.73
4	0.6827E-07	5.08	0.1690E-04	3.89
level	$\|u - u_h\|_0$	rate	$\|u - \hat{u}_h\|_0$	rate
	by the P_2 CDG solution and its P_4 lift			
2	0.2062E-03	3.21	0.8681E-04	3.92
3	0.2533E-04	3.02	0.2758E-05	4.98
4	0.3198E-05	2.99	0.8457E-07	5.03

10. CONCLUSION

The confirming discontinuous Galerkin method is an effective computational method as it produces solutions two orders in convergence above that of all other discontinuous Galerkin methods. In addition to the standard simplex and cubic meshes, the method works on general polygonal and polyhedral meshes.

11. ETHICAL STATEMENT

11.1. **Compliance with Ethical Standards.**

The submitted work is original and is not published elsewhere in any form or language.

TABLE 9.9. Error profile for solving (9.2) on 3D grids shown in Figure 9.3.

level	$\|\Pi_k u - u_h\|_0$	rate	$\|\|\|\Pi_k u - u_h\|\|\|$	rate
	by the P_2 CDG finite element			
2	0.1398E-04	6.10	0.7851E-03	4.42
3	0.2014E-06	6.12	0.2810E-04	4.80
4	0.2950E-08	6.09	0.9296E-06	4.92
level	$\|u - u_h\|_0$	rate	$\|u - \hat{u}_h\|_0$	rate
	by the P_2 CDG solution and its P_4 lift			
2	0.4041E-04	4.49	0.2603E-04	5.69
3	0.2631E-05	3.94	0.4367E-06	5.90
4	0.1666E-06	3.98	0.7009E-08	5.96

11.2. **Funding.**

None.

11.3. **Conflict of Interest.**

There is no potential conflict of interest .

11.4. **Ethical approval.**

This article does not contain any studies involving animals. This article does not contain any studies involving human participants.

11.5. **Informed consent.**

This research does not have any human participant.

11.6. **Availability of supporting data.**

This research does not use any existing nor author-collected data.

11.7. **Authors' contributions.**

All authors made equally contributions.

11.8. **Acknowledgments.**

None.

REFERENCES

[1] A. AL-Taweel, X. Wang, X. Ye and S. Zhang, A stabilizer free weak Galerkin method with supercloseness of order two, Numer. Meth. PDE, 37 (2021), 1012-1029.
[2] D. N. Arnold, An interior penalty finite element method with discontinuous elements. SIAM J. Numer. Anal., 19(4):742–760, 1982.

[3] M. Cui and S. Zhang, On the uniform convergence of the weak Galerkin finite element method for a singularly-perturbed biharmonic equation, J. Sci. Comput. 82 (2020), 5-15.
[4] Y. Feng, Y. Liu, R. Wang and S. Zhang, A conforming discontinuous Galerkin finite element method on rectangular partitions, Electronic Research Archive, 29 (2021), 2375-2389.
[5] R. Lin, X. Ye, S. Zhang and P. Zhu, A weak Galerkin finite element method for singularly perturbed convection-diffusion-reaction problems, SIAM J. Num. Anal., 56 (2018) 1482-1497.
[6] R. Lin, X. Ye, S. Zhang Y. Lin, X. Ye and S. Zhang, A Mixed Finite-Element Method on Polytopal Mesh, Commun. Appl. Math. Comput. 4 (2022), no. 4, 1374-1385.
[7] L. Mu, X. Ye and S. Zhang, A stabilizer free, pressure robust and superconvergence weak Galerkin finite element method for the Stokes Equations on polytopal mesh, SIAM J. Sci, Comput., 43 (2021), A2614-A2637.
[8] J. Wang, Q. Zhai, R. Zhang and S. Zhang, A weak Galerkin finite element scheme for the Cahn-Hilliard equation, Math. Comp., 88 (2019), 211-235.
[9] X. Ye and S. Zhang, A stabilizer free weak Galerkin method for the biharmonic equation on polytopal meshes, SIAM J. Numerical Analysis, 58 (2020), 2572-2588,
[10] X. Ye and S. Zhang, A conforming discontinuous Galerkin finite element method, Int. J. Numer. Anal. Model., 17 (2020), no. 1, 110-117.
[11] X. Ye and S. Zhang, A conforming discontinuous Galerkin finite element method: Part II, Int. J Numer. Anal. Model., 17 (2020), 281-296.
[12] X. Ye and S. Zhang, A conforming discontinuous Galerkin finite element method: part III, Int. J. Numer. Anal. Model. 17 (2020), no. 6, 794-805.
[13] X. Ye and S. Zhang, A conforming discontinuous Galerkin finite element method for the Stokes problem on polytopal meshes, Internat. J. Numer. Methods Fluids 93 (2021), no. 6, 1913-1928.
[14] X. Ye and S. Zhang, A stabilizer free weak Galerkin finite element method on polytopal mesh: Part III, J. Comput. Appl. Math. 394 (2021), Paper No. 113538, 9 pp.
[15] X. Ye and S. Zhang, A C0-conforming DG finite element method for biharmonic equations on triangle/tetrahedron, J. Numer. Math. 30 (2021), no. 3, 163-172.
[16] X. Ye and S. Zhang, A weak divergence CDG method for the biharmonic equation on triangular and tetrahedral meshes, Appl. Numer. Math. 178 (2022), 155-165.
[17] X. Ye and S. Zhang, Achieving superconvergence by one-dimensional discontinuous finite elements: the CDG method, East Asian J. Appl. Math. 12 (2022), no. 4, 781-790.
[18] X. Ye and S. Zhang, Order two superconvergence of the CDG finite elements on triangular and tetrahedral meshes, CSIAM Transactions on Applied Mathematics, 4 (2023), No. 2, 256-274.
[19] P. Zhu and S. Xie, Superconvergent weak Galerkin methods for non-self adjoint and indefinite elliptic problems, Appl. Numer. Math. 172 (2022), 300-314.

Department of Mathematics, University of Arkansas at Little Rock, Little Rock, AR 72204, USA.

E-mail address: xxye@ualr.edu

Department of Mathematical Sciences, University of Delaware, Newark, DE 19716, USA.

E-mail address: szhang@udel.edu